ENDOR Spectroscopy Reveals Light Induced Movement of the H-Bond from Ser-L223 upon Forming the Semiquinone ($Q_B^{-\bullet}$) in Reaction Centers from *Rhodobacter sphaeroides*[†]

M. L. Paddock,* M. Flores,[‡] R. Isaacson, C. Chang, E. C. Abresch, and M. Y. Okamura

Department of Physics, University of California, San Diego, La Jolla, California 92093

Received March 15, 2007; Revised Manuscript Received May 16, 2007

ABSTRACT: Proton ENDOR spectroscopy was used to monitor local conformational changes in bacterial reaction centers (RC) associated with the electron-transfer reaction $DQ_B \rightarrow D^{+\bullet}Q_B^{-\bullet}$ using mutant RCs capable of photoreducing Q_B at cryogenic temperatures. The charge separated state $D^{+\bullet}Q_B^{-\bullet}$ was studied in mutant RCs formed by either (i) illuminating at low temperature (77 K) a sample frozen in the dark (ground state protein conformation) or (ii) illuminating at room temperature prior to and during freezing (charge separated state protein conformation). The charge recombination rates from the two states differed greatly ($>10^6$ fold) as shown previously, indicating a structural change (Paddock et al. (2006) *Biochemistry 45*, 14032−14042). ENDOR spectra of $Q_B^{-\bullet}$ from both samples (35 GHz, 77 K) showed several H-bond hyperfine couplings that were similar to those for $Q_B^{-\bullet}$ in native RCs indicating that in all RCs, $Q_B^{-\bullet}$ was located at the proximal position near the metal site. In contrast, one set of hyperfine couplings were not observed in the dark frozen samples but were observed *only* in samples frozen under illumination in which the protein can relax prior to freezing. This flexible H-bond was assigned to an interaction between the Ser-L223 hydroxyl and $Q_B^{-\bullet}$ on the basis of its absence in Ser L223 → Ala mutant RCs. Thus, part of the protein relaxation, in response to light induced charge separation, involves the formation of an H-bond between the OH group of Ser-L223 and the anionic semiquinone $Q_B^{-\bullet}$. These results show the flexibility of the Ser-L223 H-bond, which is essential for its function in proton transfer to reduced Q_B.

Conformational changes in protein structure associated with electron-transfer reactions play an important role in stabilizing the resultant charge separated state and determining the rates of electron transfer (*1*−*3*). In photosynthetic bacteria, reaction centers (RCs[1]) perform the initial photochemical reactions in photosynthesis (see, e.g., refs *4* and *5*) resulting in the light induced reduction of a bound quinone, Q_B. The reduction of Q_B clearly demonstrates the influence of conformational dynamics on electron transfer. The overall reaction is shown by the solid curves in Figure 1. The first step is the initial photochemistry, a rapid ($\tau = 10^{-10}$ s) light induced electron transfer from a electron donor species D (a bacteriochlorophyll dimer) along the A-branch (one of two pseudo-symmetric pathways) through a series of acceptor molecules bacteriochlorphyll, B_A, and bacteriopheophytin, H_A, to a tightly bound quinone, Q_A (Figure 1). This is followed by a slower ($\tau = 10^{-4}$ s) electron transfer from $Q_A^{-\bullet}$ to a substrate quinone, Q_B (for a review see ref *8*). The rate of the electron-transfer reaction $Q_A^{-\bullet}Q_B \rightarrow Q_AQ_B^{-\bullet}$, $k_{AB}^{(1)}$, is coupled to protein dynamics as shown by several experimental observations (for a review see ref *9*). First, the rate of reaction is dependent on protein structure as illustrated by the effects of cross-linking (*10*), embedding in a polymer matrix (*11*), and hydration (*12*). Second, the rate is independent of the driving force (*13*), showing that electron transfer is not the rate-limiting step, indicating a conformational gating mechanism. Third, large differences in the rate of electron transfer at cryogenic temperature were found depending upon whether RCs are frozen in the light or in the dark, indicating that a structural change between the neutral and charge separated states is important for electron transfer (*14*, *15*). In the present study, we use ENDOR spectroscopy (electron nuclear double resonance) (see, e.g., *16* and *17*) to examine the differences in local structure near Q_B between the neutral and charge separated states trapped at cryogenic temperatures in order to understand the structural changes associated with the reduction of Q_B that may contribute to the conformational gating of electron transfer.

Studies conducted on protein samples frozen at cryogenic temperatures served to elucidate the importance of conformational effects on reaction dynamics. In early studies, large differences in transfer rates were observed between RCs frozen in the light or in the dark (*14*, *15*, *18*). For RCs frozen in the dark and illuminated at cryogenic temperatures, the reaction $k_{AB}^{(1)}$ became slower as the temperature decreased and did not appreciably occur below 150 K. However, if RCs were illuminated during the freezing process in the

[†] This work was supported by NIH Grant GM 41637.

* To whom correspondence should be addressed. Phone: (858) 534-2504. Fax: (858) 822-0007. E-mail: mpaddock@physics.ucsd.edu.

[‡] Current address: Max-Planck Institut für Bioanorganische Chemie, Stiftstrasse 34-36, D-45470 Mülheim an der Ruhr, Germany.

[1] Abbreviations: RC, reaction center; D, primary donor, dimer of bacteriochlorophylls; Q_A, primary quinone electron acceptor; Q_B, secondary quinone electron acceptor; $k_{AB}^{(1)}$, rate of *first* electron transfer *from* $Q_A^{-\bullet}$ to Q_B; $k_{AB}^{(2)}$, rate of *second* electron transfer *from* $Q_A^{-\bullet}$ to $Q_B^{-\bullet}$.

10.1021/bi7005256 CCC: $37.00
Published on Web 06/23/2007

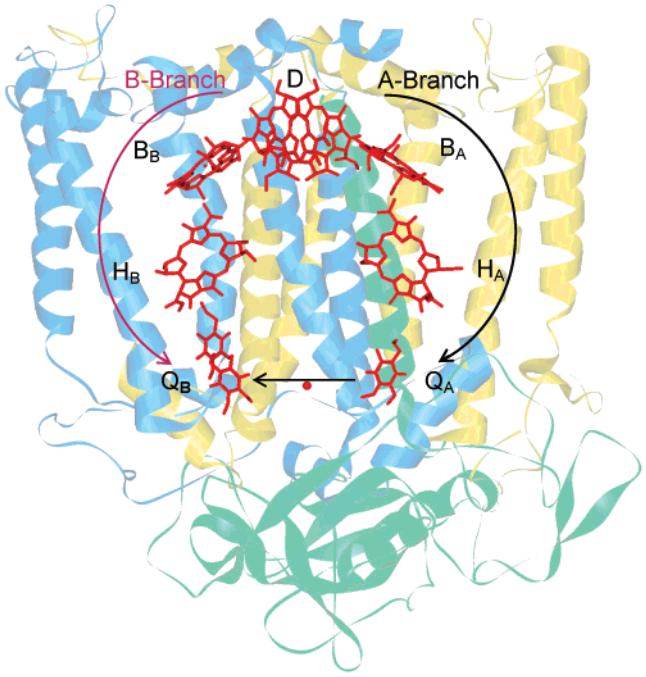

FIGURE 1: Structure of cofactors embedded within the RC protein matrix (pdb ID code 1AIG, ref *6*). The normal path for electron transfer to Q_B occurs predominantly along the A-branch from D to Q_A then Q_B (solid black arrows). The nearly symmetric cofactors along the B-branch are normally inactive in electron transfer. However, direct electron transfer to Q_B along the B-branch (red lines) can be observed in Quint RCs (B-branch mutant used in this work), which lack Q_A and have mutations that bias the electron transfer through the B-branch (*7*).

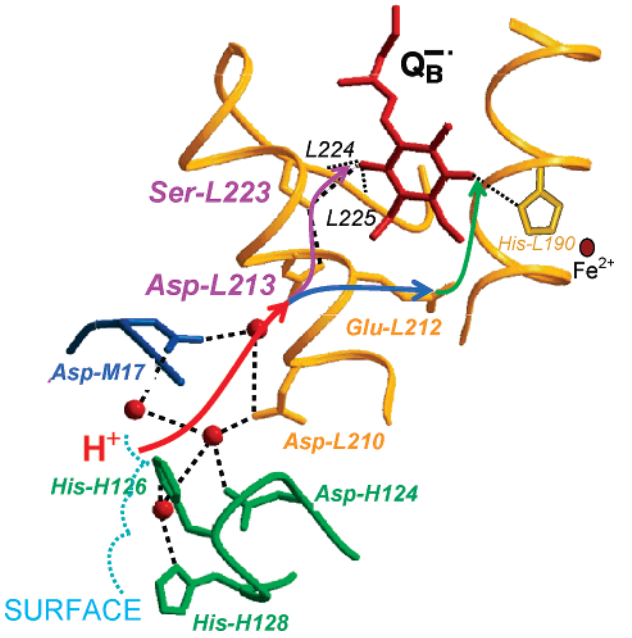

FIGURE 2: Partial structure of the RC showing the catalytic Q_B site and the proton-transfer pathways connecting it to the surface (pdb ID code 1AIG, ref *6*) showing the Q_B molecule (red); residues within H-bonding distance, His-L190 and Ser-L223 (yellow); residues that form part of the proton-transfer pathways, Asp-L213 and Asp-L210 (yellow), Asp-M17 (blue), and His-H126 and His-H128 (green); and internal bridging water molecules (red spheres) identified in the DQ_B and/or $D^{+\bullet}Q_B^{-\bullet}$ structures (pdb ID codes 1AIG and 1AIJ). Also shown are part of the subunit backbones of the L subunit (yellow), M subunit (blue), and H subunit (green) and the non-heme Fe^{2+} (rust sphere) that is replaced with the diamagnetic Zn^{2+} in this work. Closest H-bonding partners are connected via dotted lines. The potential H-bonds to the backbone are labeled with the corresponding amino acid positions, L224 and L225. The arrows represent the general flow of protons (H^+) through the pathways with the colors distinguishing different steps that occur during the photocyclic reduction of Q_B to Q_BH_2. Ser-L223 and Asp-L213 (names highlighted in magenta) are key residues discussed in this work.

$D^{+\bullet}Q_B^{-\bullet}$ state and the charges were allowed to recombine without thawing, photochemical electron transfer at cryogenic temperatures was observed (*15*, *18*), showing that a change in a structure has occurred between the neutral state and the charge separated state. The X-ray crystal structure of RCs frozen in the light ($Q_B^{-\bullet}$) and frozen in the dark (Q_B) showed a large change in the position of the quinone head group. $Q_B^{-\bullet}$ was displaced by ~5 Å to a proximal position from the prevalent distal position observed for Q_B. In this proximal position, $Q_B^{-\bullet}$ could form four H-bonds to protein groups (Figure 2) (*6*).

The large change in the position of the quinone head group suggested that the movement of Q_B from the distal to the proximal position is a possible mechanism for conformational gating of the electron transfer to Q_B (*8*, *9*). Arguments against this process being rate limiting were the finding that the rate was independent of the tail length of the quinone molecule (*13*, *19*) and the finding that a mutant having Q_B bound in the proximal site retained a slower gated rate (*20*). In addition, infrared studies suggest that at room temperature Q_B is predominantly in the proximal site (*21*). These results suggested that additional conformational changes besides the quinone movement must contribute to the reaction.

An additional model for the conformational gate is that the protein structure alters the free energy of electron transfer from $Q_A^{-\bullet}$ to Q_B. In this model, the free energy is unfavorable with the protein in the unrelaxed structure near Q_B (RCs frozen in the dark). It becomes favorable as the protein and solvent relax into a conformation that stabilizes the charge separated state (reflected in the RCs frozen in the light). In order to test this hypothesis, we have studied the reduction of Q_B using RCs mutants that are modified to allow direct electron transfer to Q_B from the B-branch bacteriopheophytin located close to Q_B (see red curved arrow in Figure 1). Using the higher driving force for electron-transfer, it was possible to form the charge separated state $D^{+\bullet}Q_B^{-\bullet}$ in RCs frozen in the less thermodynamically favorable unrelaxed conformation of the dark (*7*). In this way, it was possible to monitor the differences between the stability of the charge separated $D^{+\bullet}Q_B^{-\bullet}$ states and measure the EPR and ENDOR spectra for RCs frozen in the unrelaxed (dark frozen) and relaxed (light frozen) conformations.

In a previous article (*7*), we showed that the lifetime of the charge separated state $D^{+\bullet}Q_B^{-\bullet}$, which is dependent on the stabilization of $Q_B^{-\bullet}$, was dramatically effected by the conditions of its formation. In a dark frozen sample (77 K), charge separation occurred in a minor fraction (~30%) of the sample with a lifetime of ~6s. In a sample frozen under illumination, $D^{+\bullet}Q_B^{-\bullet}$ was formed in the entire sample with a lifetime exceeding 10^7s (77 K) (*7*). Thus, the protein response, which was prevented by freezing in the dark in the former sample, resulted in a $> 10^6$-fold difference in the lifetime at 77 K. For simplicity, we shall refer to samples prepared in that manner as unrelaxed (frozen in the dark) and relaxed (in which illumination occurred prior to freezing, allowing the protein to respond/relax). In those studies, $Q_B^{-\bullet}$

were formed by electron transfer from $BPhe_B$, in a mutant designed to increase the efficiency of B-branch electron transfer (described in ref *22*). This mutant RC carried the Ala-M260 → Trp replacement designed to remove Q_A (*22*−*24*), thereby creating an RC system without an admixture of $Q_A^{-\bullet}$.

In this work, we extend the previous EPR studies by using ENDOR spectroscopy at 35 GHz to examine the local structure near $Q_B^{-\bullet}$ in both the relaxed and unrelaxed protein conformations. ENDOR spectroscopy can be used to determine positions of protons that are not observable with X-ray crystallography and is particularly well suited for the examination of detailed interactions between a radical cofactor and its protein surrounding (see, e.g., ref *25*). Interactions between the magnetic moment of the unpaired electron of the radical and magnetic moments of protons (nuclei) from the surrounding protein are detected with a spatial resolution approaching 0.03 Å (see, e.g., ref *26*). Thus, ENDOR can provide a precise measure of the binding position and details on the interactions of $Q_B^{-\bullet}$ in its binding pocket (Figure 2). At 35 GHz, the ^{1}H ENDOR signals resulting from interactions between $Q_B^{-\bullet}$ and the protein are spectrally separated from those associated with $D^{+\bullet}$. The ^{1}H ENDOR spectra of the relaxed and unrelaxed states were measured and differences between them discussed, and the implications for the catalytic functions (i.e., reduction and protonation) of Q_B are also discussed.

MATERIALS AND METHODS

Construction and Purification of the Quintuple B-Branch Mutant RCs. The construction and purification of the B-branch mutant was previously described (*22*). The mutant RC contained the following changes: GCC → TGG (Ala-M260 → Trp), CTG → CAC (Leu-M214 → His), TAC → TTC (Tyr-M210 → Phe), GGT → GAC (Gly-M203 → Asp), TTC → TAC (Phe-L181 → Tyr), and in one mutant TCG → GCC (Ser-L223 → Ala). RCs were purified as previously described (*27*).

Biochemical Zn^{2+} Replacement. To perform EPR and ENDOR spectroscopic studies on $Q_B^{-\bullet}$, the high spin Fe^{2+} was removed and replaced with diamagnetic Zn^{2+} as described by Debus et al. (*28*) and as modified by Utschig et al. (*29*). Protonated quinone/semiquinone was removed from the Q_B site by incubating for 30 min in 100 mM Caps at pH 11 and 100 μM ferricyanide (to oxidize the fraction of $Q_B^{-\bullet}$ present in the dark), and 2% LDAO and 100 mM *o*-phenanthroline (to displace UQ_{10}). The RCs were bound to a DEAE column and rinsed with 10 column volumes of 10 mM Caps at pH 11, 10 μM ferricyanide, and 100 mM *o*-phenanthroline, and then with 10 column volumes 10 mM Tris at pH 8, 0.025% LDAO, and 1 mM EDTA. The B-branch mutant RCs were reconstituted with ~3-fold excess of deuterated UQ_{10} in 1% LDAO to occupy the Q_B site followed by dialysis against TMK (2 mM Tris-HCl at pH 8, 0.04% β-D-maltoside, and 5 mM KCl). The Q_B site of the native RC was reconstituted with 10-fold excess of deuterated UQ_{10} in 1% LDAO, diluted 4-fold, and concentrated in an Amicon concentrator. The concentrated material was then used to make EPR and ENDOR samples with the intent of minimizing incubation that would allow the exchange of protonated quinone from the Q_A site.

35GHz EPR and ^{1}H ENDOR Measurements. EPR and ENDOR spectroscopy were performed at a microwave frequency of 35 GHz at $T = 77$ K as previously described (*30*). For the B-branch mutant RC, two parallel samples were made from the same RC material (at ~100−700 μM RC). One was frozen in liquid nitrogen in the dark. The other was illuminated by a projector (~1 W/cm^2, ~5 s) and frozen in liquid nitrogen under illumination. A similar projector was used to illuminate the sample in the magnetic resonance cavity to generate the charge separated state in the sample frozen in the dark. For the native RC, the $D^{+\bullet}Q_A^{-\bullet}$ state was produced by chemical reduction as described (*30*). The $D^{+\bullet}Q_B^{-\bullet}$ state was produced by illuminating with a projector (~1 W/cm^2, ~1 s) and freezing in liquid nitrogen under illumination.

THEORY

ENDOR spectroscopy utilizes radio frequency radiation to excite nuclear magnetic resonance transitions that are detected by changes in the EPR signal of an interacting electron spin (*16*, *17*). ENDOR spectra are plots of the EPR signal amplitude versus the frequency of the applied radio frequency radiation used to modulate the proton spin. The simplest ENDOR spectrum of a single proton interacting with an electron spin for a molecule in a fixed orientation such as that in a crystal consists of two lines centered symmetrically around the free proton frequency, υ_{free}, where A is the hyperfine coupling due to the interaction between the nuclear spin and electron spin (eq 1). The larger the coupling, the larger the interaction and most likely the smaller the distance between the proton and electron spin.

$$\nu = \nu_{free} \pm \frac{A}{2} \tag{1}$$

where ν is the peak frequency, ν_{free} the free proton frequency, and A the hyperfine coupling constant.

The ENDOR spectra due to interactions between H-bonded protons and the semiquinone have been extensively described (*25*). In its simplest form, the ENDOR spectra from H-bonded protons arise from the magnetic dipole interaction between the nuclear spin of the proton with the electron spin at the H-bonded oxygen on the quinone. The interaction is anisotropic, that is, it depends on the orientation of the magnetic field vector with respect to the H-bond direction. For a randomly oriented sample such as that used in this study, the powder pattern ENDOR spectrum due to a single proton shows resonances at many frequencies because of the different orientations of the molecule in the magnetic field. At the magnetic field position corresponding to g_y, the spectrum corresponds to a two-dimensional powder-type spectrum, with weighted contributions mainly from all *in-plane* directions, providing little field selection (see, e.g., ref *26*). The major features of the spectra are four peaks with two peaks below the free proton frequency and two peaks above the free proton frequency symmetrically spaced around the free proton frequency. The larger coupling, $A_{||}$, is from an orientation in which the magnetic field is parallel to the H-bond direction, and the smaller coupling, $A_\perp$, is from an orientation in which the magnetic field is perpendicular to the H-bond direction. For the case where the interaction is due to a magnetic dipolar interaction alone (i.e., no isotropic

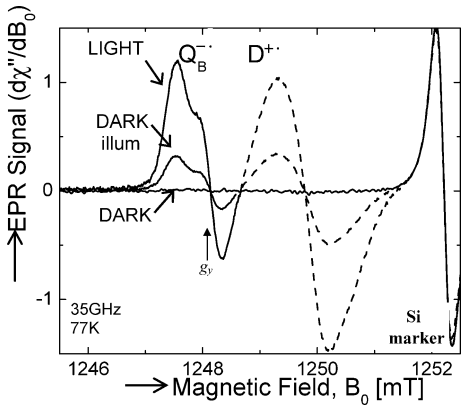

FIGURE 3: EPR spectra (35 GHz) ($d\chi''/dB_0$) of $D^{+\bullet}Q_B^{-\bullet}$ in the dark frozen sample before (DARK) and after illumination (DARK illum) and in the sample frozen under illumination (LIGHT). The EPR peak positions (principal *g*-values) are the same in the DARK and LIGHT samples; the amplitude was ~5-fold smaller in the DARK illum sample because of the minor fraction in which the $D^{+\bullet}Q_B^{-\bullet}$ state can be generated (*7*). The RCs were chemically treated to replace the Fe^{2+} with Zn^{2+} to allow observation of $Q_B^{-\bullet}$, which would otherwise be broadened by the spin of the Fe^{2+} (*33*). At 35 GHz, the low field region of the EPR spectrum arises from $Q_B^{-\bullet}$ (as labeled on left side of traces) and is spectrally separated from that of $D^{+\bullet}$ (as labeled in middle of traces); a Si marker line is located on the far right. The lifetime of charge separated state was the same as that observed in Fe^{2+} containing RCs and the same as that observed at 9 GHz (*7*). (Conditions: [RC] ~100 μM, ID of EPR tube = 0.2 cm, ν = 35 GHz, 77 K; 16 traces were averaged.)

coupling due to covalency), the principal values are related by a factor of 2 such that $A_{\|} = -2A_{\perp}$ (*25*). For this simple case, the value of the hyperfine coupling is given by eq 2 as follows:

$$A = \frac{79.2\rho}{r^3}(3\cos^2\delta - 1)\ [\text{MHz}] \qquad (2)$$

where r is the distance in Å between the proton and oxygen, ρ is the spin density on the oxygen, and δ is the angle between the magnetic field and the H-bond direction. For $A_{\|}$, $\delta = 0$, and for $A_{\perp}$, $\delta = 90°$. The simple point dipole model adequately describes some systems such as (within 5%) benzosemiquinones in solution (see, e.g., ref *31*). However, recent studies of the interaction of $Q_A^{-\bullet}$ with its two H-bonds in the RC showed that this simple picture must be modified because of the interaction with the His-Zn^{2+} proton due to a significant isotropic coupling with the semiquinone. The point dipole approximation can also fail for the case where the direction of the H-bond significantly deviates from the plane of the quinone ring (*26*, *32*).

RESULTS

EPR Spectra in the Frozen State at 77 K. The signals from the charge separated $D^{+\bullet}Q_B^{-\bullet}$ states were monitored by EPR spectroscopy (35 GHz, 77 K) using the quintuple B-branch mutant RC (Quint RCs) (containing Zn^{2+}/deuterated Q_{10}) frozen in the light or frozen in the dark. In the samples frozen under illumination, an EPR signal was observed because of the charge separated state $D^{+\bullet}Q_B^{-\bullet}$ (Figure 3, LIGHT). At 35 GHz, the signal due to $Q_B^{-\bullet}$ at low field was completely separated from the signal at higher field due to $D^{+\bullet}$ (Figure 3) allowing ENDOR spectra of the quinone to be made with no contribution from the donor. The EPR signal was stable at 77 K and does not decay for $\tau > 10^6$ s. For the sample frozen in the dark, no EPR signal was initially observed (Figure 3, DARK). However, an EPR signal due to the charge separated state $D^{+\bullet}Q_B^{-\bullet}$ was formed upon illumination (Figure 3, DARK illum). The EPR signals for RCs frozen in the light and dark exhibited very similar *g* values. The light induced signal decayed in the dark with a lifetime of ~6 s as previously observed (*7*). The signal was absent in control samples (not shown) to which the Q_B site inhibitor, stigmatellin, was added showing that the signal results from $D^{+\bullet}Q_B^{-\bullet}$. Similar EPR signals were seen in Quint RCs having the mutation Ser L223 → Ala that were frozen in the light. However, no light induced EPR signals were seen in these mutant RCs that were frozen in the dark.

^{1}H ENDOR Spectra of $Q_B^{-\bullet}$ in the Frozen State at 77 K in the B-Branch Mutant RC. To investigate local structural changes that occur upon charge separation, ^{1}H ENDOR spectra of $Q_B^{-\bullet}$ were measured in the Quint RC frozen in the light and frozen in the dark. In addition, the ENDOR spectrum of Quint RCs having a mutation to the H-bond donor residue Ser L223 → Ala was measured in order to help identify ENDOR lines. The samples contained deuterated quinone. Thus, the proton ENDOR lines due to the protons on the quinone are eliminated, and only ENDOR lines contributed by the protein and solvent protons are expected. The samples were monitored at the magnetic field position corresponding to g_y (see arrow in Figure 3), which provided the largest $Q_B^{-\bullet}$ ENDOR signals with minimal contribution from $D^{+\bullet}$.

The complete ENDOR spectra centered around the free proton frequency are displayed in Figure 4A. Lines with larger splittings (|A| > 3 MHz) are due to hydrogen bonding interactions (H-bonds) between the oxygen atoms of $Q_B^{-\bullet}$ and protons from the nearby protein (*25*). Lines with smaller splittings (|A| < 3 MHz) due to weaker interactions of the quinone with more distant protons are seen in the matrix region (matrix). A few changes occurred in the matrix region. In particular, the lower frequency edge of the matrix region (52.2−52.5 MHz) differed between the Quint (light) and Quint (dark), and between these and the mutant RC with the additional SAL223 replacement. Assignments for these lines were not attempted because such lines are the result of interactions with numerous more distant protons. In addition, not all of the matrix protons were exchangeable, indicating contributions to the spectra of nonexchangeable side chain protons.

The low frequency side ENDOR spectra in the H-bonding region for the three samples are shown in Figure 4B. In the ENDOR spectrum of Quint RC frozen in the light, we tentatively assigned three pairs of lines to the $A_{\|}$ and $A_{\perp}$ components of three H-bonds to $Q_B^{-\bullet}$. These are shown in Figure 4B, LIGHT labeled (1, 1′), (2, 2′) and (3, 3′), respectively. The smaller peaks (1, 2, 3) were attributed to the parallel ($A_{\|}$) components of the three H-bond hyperfine coupling tensors. The higher intensity lines (1′ and 3′) and shoulder (2′) were attributed to their respective perpendicular ($A_{\perp}$) components. The amplitude of all of the H-bonding lines were all diminished when the solvent was changed to D_2O (48 h) showing that the protons were exchangeable (data not shown) as expected. It is likely that peaks 3 and 3′ are composed of overlapping signals from two different protons

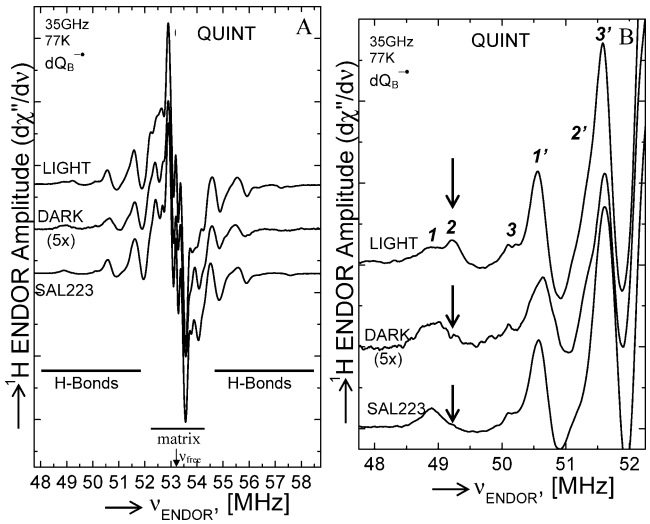

FIGURE 4: ENDOR spectra of $Q_B^{-\bullet}$ in the B-branch mutant (QUINT) samples frozen under illumination (LIGHT), frozen in the dark, and illuminated (DARK), and in a mutant containing the additional Ser-L223 → Ala (SAL223) replacement. (A) At the magnetic field position corresponding to g_y, proton nuclei that couple to the spin of $Q_B^{-\bullet}$ result in two pairs of lines symmetrically shifted from the free proton frequency. The principle values of the hyperfine coupling interaction, $A_{||}$ and $A_{\perp}$, are obtained from the frequency difference between symmetrically related lines (see text). At the bottom, the black bars indicate the H-bonding region where peaks associated with H-bonds between $Q_B^{-\bullet}$ and the protein are observed; the black bar on the bottom indicates the matrix region, which is composed of numerous more weakly coupled protons; an arrow indicates the free proton frequency, corresponding to the position at which a line resulting from an uncoupled proton would appear (i.e., with no hyperfine interaction). Note the overall similarity of the traces, in particular in the region in which peaks due to H-bonds are observed. The amplitude of the dark sample was increase 5-fold because only a fraction of the sample undergoes charge separation, to allow a better comparison of the ENDOR signals. (B) Expansion of the ENDOR spectra of $Q_B^{-\bullet}$ focusing on left H-bonding region from part A. Note that the majority of the peaks (labeled in pairs *1* and *1′*, *2* and *2′*, and *3* and *3′*) are at the same position in all of the samples; the peaks are slightly broader in the sample frozen in the dark. This indicates that the binding position of $Q_B^{-\bullet}$ with respect to the local protein is the same in all of the samples. There is one exception indicated by an arrow and labeled *2* that is present only in the sample frozen under illumination (LIGHT); it is not present in the sample frozen in the dark (DARK), nor in the sample with the additional Ser-L223 → Ala replacement (SAL223). (Conditions: [Zn-RC(dQ)] ~0.7 mM, ID of EPR tube = 0.2 cm, ν = 35 GHz, and 77 K; up to 80,000 traces were averaged.)

on the basis of the previous site-directed mutagenesis experiments on Native RCs (*34*).

The ENDOR spectrum of $Q_B^{-\bullet}$ in the H-bonding region in RCs frozen in the dark was similar to that of RCs frozen in the light, indicating that almost all of the H-bonds are present in both cases (Figure 4B, DARK). However, peak 2 (and 2′), indicated by the arrow in Figure 4B, is present in the sample frozen in the light but is not present in the sample frozen in the dark. To help identify the missing peak, the ENDOR spectrum of the mutant RC containing the additional Ser-L223 → Ala replacement (SAL223) was measured. The ENDOR spectrum of the SAL223 mutant in the H-bond region is similar to that of the Quint RCs but lacks peak 2 (and 2′) (Figure 4B, SAL223). The absence of peak 2 in the SAL223 ENDOR spectrum shows that this peak is due to the H-bond from Ser L223.

^{1}H ENDOR Spectra of $Q_B^{-\bullet}$ in the Native RC. We wished to assess the similarity of the native $Q_B^{-\bullet}$ ENDOR spectra with that measured for the B-branch mutant for samples frozen under illumination. However, it was difficult to obtain a pure ^{1}H ENDOR spectrum of $Q_B^{-\bullet}$ of the native RC because of contributions from $Q_A^{-\bullet}$ in the sample due to the intrinsic equilibrium between $Q_A^{-\bullet}$ and $Q_B^{-\bullet}$ and a fraction of RCs that lack Q_B. In order to remove the spectrum of $Q_A^{-\bullet}$ from the native ENDOR spectrum, we focused on the matrix region, which was expected to be very similar because it is composed of contributions of more distant protons that are essentially structurally the same in the native and mutant RCs (*35*). Because of the reconstitution procedure, Q_A almost exclusively contained the native (non-deuterated) Q_{10} (spectrum shown in Figure 5A). A fraction of the $Q_A^{-\bullet}$ spectrum was subtracted from the native OBS spectrum giving a DIFF spectrum (Figure 5A, OBS) that resembled that of the B-branch mutant $Q_B^{-\bullet}$ in the matrix region (Figure 4A, quintuple LIGHT). In particular, the peaks in the matrix region near 52.6 and 53.8 MHz were diagnostic of the $Q_A^{-\bullet}$ contribution to the observed spectrum. The resultant difference spectrum is shown labeled as DIFF in Figure 5. This spectrum revealed peaks that were analogous to those observed in the ^{1}H-ENDOR $Q_B^{-\bullet}$ spectrum of the B-branch mutant RC frozen under illumination (Figure 4, LIGHT). In particular, a peak analogous to that assigned to the hydroxyl group of Ser-L223 (arrow) was observed in the native sample (Figure 5B); the slight shift in the position of the peak near 49.3 MHz could be the result of a small (<0.1Å) increase in the length of the H-bond in the native RC.

DISCUSSION

In this work, we used ENDOR spectroscopy to investigate the local changes in the protein that occur near Q_B upon its reduction in the photosynthetic bacterial RC from *Rhodobacter (Rb.) sphaeroides*. Changes were observed that could contribute to the >10^6-fold greater lifetime of the $D^{+\bullet}Q_B^{-\bullet}$ state formed by freezing under illumination compared to that formed by illumination of a sample frozen in the dark. The observed changes, the implications on the binding position of the quinone and its properties, and the possible functional relevance for facile proton transfer of the observed changes are discussed below.

Reducible Q_B Bound to the Proximal Position. The ^{1}H-ENDOR spectra of $Q_B^{-\bullet}$ in the H-bonding region in Quint RCs frozen in the light and in the dark (Figure 4B), and in Native RCs (Figure 5B) were very similar (with the exception of a single peak that is absent in RCs frozen in the dark). The similarity in the peak positions indicated that most of the H-bonds to the semiquinone were similar in all three RCs. Because the semiquinone $Q_B^{-\bullet}$ in native RCs was found to be in the proximal position in the X-ray crystal structure for the Native RC (*6*, *36*), we conclude that in all cases $Q_B^{-\bullet}$ was located in the proximal binding site.

$Q_B^{-\bullet}$ Bound to the Distal Position Was Not Observed. For the Quint RC frozen in the dark, it has been shown that only a fraction (~30%) are in an active configuration capable of photochemical reduction of Q_B (*7*). The results from this study indicated that this active configuration is one in which Q_B is bound in the proximal site. The activity of Q_B in the proximal site is probably due to the strong effect of the

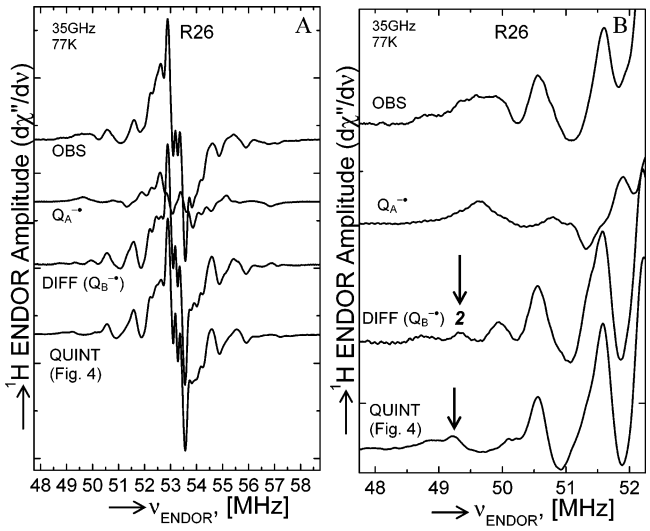

FIGURE 5: ENDOR spectra of $Q_B^{-\bullet}$ and $Q_A^{-\bullet}$ in the native (R26) RC frozen under illumination. (A) Shown are the complete ENDOR spectra within 12 MHz of the free proton frequency. The top trace shows that observed (OBS) for a native sample excited with a single saturating laser flash. The Q_B site was occupied with deuterated UQ_{10}. This trace includes an admixture of some $Q_A^{-\bullet}$. The spectrum of $Q_A^{-\bullet}$, measured in a sample lacking Q_B, is shown in the second trace; because of the reconstitution procedure, the Q_A site almost exclusively contained the native (non-deuterated) UQ_{10}. The contribution of $Q_A^{-\bullet}$ was subtracted from the observed trace to yield the spectrum of $Q_B^{-\bullet}$ shown as the third trace (DIFF ($Q_B^{-\bullet}$)). The scaling factor for the amount of $Q_A^{-\bullet}$ in the observed trace was determined by matching the matrix region of the DIFF ($Q_B^{-\bullet}$) with that of the quintuple $Q_B^{-\bullet}$ (QUINT) obtained by freezing under illumination (from Figure 4). Because the matrix peaks result from protons located further from the semiquinones, they should be less sensitive to possible local structural changes. For example, the peak near 52.5 MHz, which is a prominent matrix peak of $Q_A^{-\bullet}$, was used to determine the relative amount of $Q_A^{-\bullet}$ to be subtracted from the observed spectrum. The difference spectrum better matched other parts of the matrix region, indicating that the subtraction was appropriate. Without knowledge of the quintuple $Q_B^{-\bullet}$, the scaling factor for the amount of $Q_A^{-\bullet}$ in the observed spectrum would have been difficult (if not impossible) to determine. (B) Expanded view of the left side emphasizing the H-bonds. Note the similarity of the peaks in the native $Q_B^{-\bullet}$ shown in the third trace from the top (DIFF ($Q_B^{-\bullet}$)) and those from the Quintuple mutant in which $Q_A^{-\bullet}$ cannot be formed. Highlighted with an arrow is the peak attributed to the hydroxyl group of Ser-L223, which is also present in the spectrum of the native sample. The small shift in position may indicate a slight difference in distance of the magnitude of ~0.02 Å. Small shifts are also observed in the position of many of the smaller amplitude peaks. Overall, the native $Q_B^{-\bullet}$ is within uncertainty the same as that of the quintuple $Q_B^{-\bullet}$. In particular, the H-bond from Ser-L223 (labeled *2*) is present in the native $Q_B^{-\bullet}$ spectrum. (Conditions: [Zn-RC(dQ)] ~0.7 mM, ID of EPR tube = 0.2 cm, ν = 35 GHz, and 77 K; up to 30,000 traces were averaged.)

H-bonds in stabilizing the negative charge on the semiquinone in the charge separated state. The X-ray crystal structure of Quint RCs frozen in the dark showed that the predominant position of Q_B was in the distal site (*22*). Thus, these results show that Q_B in the distal site is apparently not stably reduced. It was either not reduced efficiently by $H_B^{-\bullet}$ or was reduced but rapidly recombined resulting in a small (unobserved) steady-state population.

Assignment of the Mobile Proton upon Q_B Reduction to Ser-L223. Although the majority of the ENDOR lines in the H-bonding region were the same between the Quint (light) and Quint (dark), there was one peak indicated by an arrow (labeled *2*) that was absent in the Quint (dark) (Figure 4B). Most of the H-bonds (from NH protons from backbone peptides of His) to the quinone bound in the proximal site are rigidly fixed in the protein structure, and their positions can be deduced from the X-ray crystal structure. In contrast, the hydroxyl group from Ser L223 can serve as an H-bond donor to either Q_B or to Asp L213 (Figure 2). Thus, the H-bond from Ser L223 cannot be determined by X-ray crystallography. The definitive assignment of the ENDOR line *2* to the hydroxyl proton of Ser-L223 came from studies on the effects of mutations on the observed spectrum. In the mutant RC with the additional Ser-L223 → Ala replacement, the peak was absent (see arrow in Figure 4B). From this result, we concluded that this peak is due to the interaction from the hydroxyl proton of the Ser side chain.

The absence of peak *2* assigned to Ser L223 in the unrelaxed RC was attributed to a change in the position of the proton because of the switch in the H-bond from $Q_B^{-\bullet}$ to Asp L213. Because ENDOR is extremely sensitive to distance, an increase in the distance between the oxygen atom of $Q_B^{-\bullet}$ and the proton of as small as ~1 Å would shift the peak from the H-bonding region to the matrix region (Figure 4A). Although the ENDOR spectrum in the matrix region is very congested and difficult to analyze, there are changes that could be due to movement of the H-bonded proton, for instance, the low-frequency peak at 52.25 MHz. Thus, the proton responsible for the ENDOR line had a hyperfine coupling of $A_{||} = 8.0$ MHz (±5%) in Quint (light) (i.e., the line is shifted ±4.0 MHz from the free proton frequency of 53.25 MHz, to 49.25 MHz on the low frequency side shown in Figure 4B) and a smaller coupling of most likely $A_{||} < 2$ MHz in Quint (dark).

For a proton in a typical hydrogen bond, the point dipole approximation can be used to estimate the H-bonding distance from the value of the hyperfine interaction (eq 2). Using the apparent value of $A_{||} = 8.0$ MHz and previously determined values for the spin density ($\rho = 0.18$) at the oxygen atom nearest Ser-L223 (see, e.g., ref *25*), we obtain from eq 2 a distance of 1.5 Å from the proton to the oxygen atom. Because this equation is known to underestimate the distance by ~0.2 Å for the H-bonds to $Q_A^{-\bullet}$ (*26*, *32*), the real distance is slightly longer and closer to 1.7 Å, which is essentially an optimal hydrogen bond distance (see, e.g., ref *37*). Thus, the magnitude of the hyperfine interaction adds further support for the assignment of the line to the H-bond from Ser L223.

Ser-L223 Hydroxyl Proton ENDOR Line in the Native RC. The $Q_B^{-\bullet}$ ENDOR spectrum of the native RC was determined for the relaxed protein conformation by subtracting the contribution due to $Q_A^{-\bullet}$. The similarity of the native deconvoluted $Q_B^{-\bullet}$ spectrum in the H-bonding region (Figure 5B) to that measured in the B-branch mutant (Figure 4B) showed that $Q_B^{-\bullet}$ has essentially the same H-bond interactions in both the native and mutant RCs. In particular, the peak assigned to the H-bond from Ser L223 is present in both native and Quint RCs frozen in the light. The small changes in the position of the ENDOR peaks in the H-bonding region (~0.1−0.2 MHz) indicate slight changes in the H-bond juxtaposition (such as the change in distance as minor as ~0.02 Å). These results indicate that in the relaxed protein conformation $Q_B^{-\bullet}$ was in the proximal

position with an H-bond to Ser L223 in the native RC as well as in the Quint RC.

These results extend the previous findings by Utschig et al. (*38*) who used high field ENDOR to investigate changes in $D^{+\bullet}Q_B^{-\bullet}$ states formed by freezing under a variety of light exposure conditions, resulting in a variety of partially relaxed configurations. They obtained samples in which $D^{+\bullet}Q_B^{-\bullet}$ was inactive, that is, no observed recombination at 20 K, or active in which $D^{+\bullet}Q_B^{-\bullet}$ decayed nonexponentially in 10−100 s at 20 K and could be formed by illumination at low temperature. The former state was analogous to the relaxed $Q_B^{-\bullet}$ state reported in this work. They reported no difference between the ENDOR spectra in the matrix regions of their active and inactive states. This observation suggests that their active, that is, partially relaxed, state has ENDOR properties similar to those of the fully relaxed state.

Gating of Electron Transfer. One of the unresolved questions related to the reduction of Q_B is the nature of the conformational gate that limits its reduction via the prevalent A-branch. The sensitivity of ENDOR spectroscopy enables one to observe small changes in proton positions that are otherwise difficult to detect but possibly important for the energetics of enzymatic reactions. In this work, we observed a change in the H-bonding of $Q_B^{-\bullet}$ in response to its reduction using the quintuple mutant in which Q_B was reduced via the B-branch. Electron transfer via the B-branch has a greater driving force, thereby allowing access to states that are otherwise inaccessible. We assigned the responsive H-bond to the hydroxyl group of Ser-L223. The overall similarity to the native ENDOR spectrum suggests that these results are applicable to the native RC. An increase in the stabilization of $Q_B^{-\bullet}$ could result from the formation of an H-bond to the Ser-L223 hydroxyl group and could explain (in part) the increased lifetime of the relaxed $D^{+\bullet}Q_B^{-\bullet}$ state. However, Ser-L223 H-bond formation is not by itself the conformational gate that limits Q_B reduction via the A-branch because the observed electron-transfer rate remains very similar in a mutant in which Ser-L223 is replaced with Ala (*39*). Additional changes observed in the matrix region indicated that more distant protons have also responded to the charge separation. Further studies are needed to assign these lines to specific protons.

Effects of Protein Response on Functional Properties of Q_B. A major functional difference between the Quint RCs frozen in the dark and frozen in the light is the lifetimes of the charge separated states, which were found to be 6 s and $>10^7$ s, respectively (*7*). Similar long lived states have been observed by other authors for native RCs frozen under different illumination conditions (*15*, *18*, *38*, *40*, *41*). In principle, the longer lifetime of the long lived state frozen in the light may be due to a reduced electron-transfer rate for the back electron-transfer reaction. This could result from either a change in electronic coupling or in the driving force (*42*). Because the ENDOR spectra indicate that the location of $Q_B^{-\bullet}$ is the same for RCs frozen in the light or in the dark, it is unlikely that a change in electronic coupling alone could be large enough to account for the change in rate. A change in distance of greater than 5 Å would be required, which is inconsistent with ENDOR results. Thus, it seems that the stabilization of the charge separated state is due to a lowering in energy of the relaxed state.

Although it is tempting to ascribe the lowering in energy in the relaxed state to the switch of the Ser L223 H-bond, the H-bond energy is not sufficient to account for the observed change in the rate because we observed a long lifetime for the Quint mutant lacking Ser L223 (Figure 4). Instead, it is likely that there are many changes that contribute to charge stabilization. Alexov and Gunner (*43*), Ishikita and Knapp (*44*), and Zhu and Gunner (*45*) have provided possible molecular responses and a starting point for the discussion of molecular changes resulting from the reduction of Q_B. In addition to the stabilizing effect of forming an H-bond to $Q_B^{-\bullet}$ from Ser L223, protonation of a cluster of acids near the Q_B site could provide additional stability to the charge separated state. Furthermore, protonation of a water molecule in the Q_B region was suggested on the basis of FTIR spectroscopy (*46*). The overall stabilization is likely to be due to the sum of many contributions.

Our ENDOR results indicate the formation of an H-bond between $Q_B^{-\bullet}$ and Ser L223 at cryogenic temperatures. In contrast, FTIR studies suggest that the $Q_B^{-\bullet}$ is not H-bonded to Ser L223 at higher temperatures (>280 K) (*47*). A possible resolution to this seemingly contradictory result is that H-bonding is temperature-dependent. If the Ser L223 does not form a H-bond to $Q_B^{-\bullet}$, then it should be H-bonded to the nearby Asp-L213 (Figure 2). The H-bond to Asp L213 should be especially favorable if Asp L213 is negatively charged as suggested by kinetic measurements (*48*, *49*) and FTIR studies (*50*). The formation of an H-bond between Ser L223 and $Q_B^{-\bullet}$ at low temperature suggests that under these conditions Asp L213 is protonated. We suggest that the protonation of Asp L213 may also be present in the relaxation process (Figure 6). The protonation of Asp L213 and other carboxylic acid residues in the region may contribute to the stabilization of $Q_B^{-\bullet}$ in the charge separated state at low temperature.

Role of Ser L223 in Proton Transfer. The H-bond from Ser L223 plays a crucial role in proton transfer to $Q_B^{-\bullet}$ associated with electron transfer. The mutation of Ser L223 to Ala drastically reduces the rate of proton coupled electron transfer that has been proposed to be due to the blocking of proton transfer to $Q_B^{-\bullet}$ (*39*). The mechanism of proton transfer in biological systems is believed to occur through a chain of H-bonded groups in series via a Grothuss mechanism (*8*, *51*). The Grothuss mechanism consists of two steps: (1) the transfer of protons across the H-bonds and (2) the rotation of the H-bond from one H-bond acceptor group to another to re-establish the starting H-bond pattern. The proton transfer to $Q_B^{-\bullet}$ can be seen as an extension of the proposed relaxation process in Figure 6. The rotation of the H-bond from Asp L213 to $Q_B^{-\bullet}$ is followed by proton transfer, producing the protonated semiquinone $Q_BH^{\bullet}$. In the mechanism for proton coupled electron transfer to reduced Q_B (*52*, *53*), the protonated semiquinone is not a stable species but is an intermediate state, present with low probability, that serves as the acceptor for electron transfer from $Q_A^{-\bullet}$. The protonation step is crucial to establish a favorable driving force for electron transfer. Overall, the proton equilibrates rapidly and is not rate limiting. The rapid rate of proton transfer to $Q_B^{-\bullet}$ is greatly facilitated by the

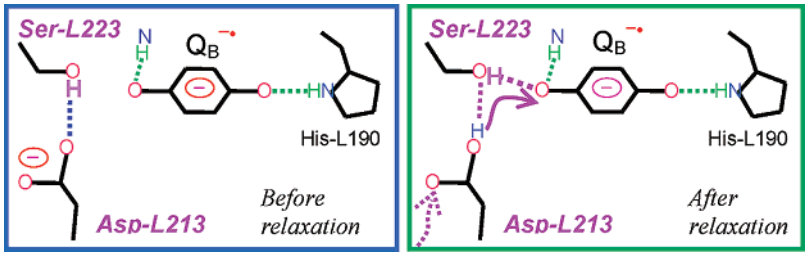

FIGURE 6: Model of the Q_B site to explain the observed low temperature (77 K) ENDOR spectra. On the left is the model for the active fraction of the frozen-in-the-dark sample in which Q_B is bound in the proximal site with the protein in the ground state conformation, that is, prior to charge separation. Upon illumination, the $D^{+\bullet}Q_B^{-\bullet}$ state is formed and detected with EPR and ENDOR spectroscopy. Because the sample is frozen, the normal protein relaxation to the formation of $Q_B^{-\bullet}$ is inhibited and is thus termed the *unrelaxed* conformation. On the right is the model for the sample frozen under illumination in which $Q_B^{-\bullet}$ is bound in the proximal site with the protein in the excited-state conformation, i.e., following charge separation. Because the charge separated state is formed at higher temperatures (298 K), the protein can respond to the charge separation prior to freezing, and consequently, the protein is in the *relaxed* conformation. The major difference observed in the ENDOR spectra is the H-bond between Ser-L223 and $Q_B^{-\bullet}$, which is present only in the *relaxed* conformation at 77 K. Calculations suggest that this H-bond occurs when Asp-L213 becomes protonated (*43*, *44*). These changes indicate the formation of an H-bond network that could promote proton transfer as indicated by the arrows.

switching capability of the H-bond from Ser L223 (*8*, *43*, *54*, *55*).

SUMMARY AND CONCLUSIONS

In this work, we investigated the structural changes near the reduced quinone $Q_B^{-\bullet}$ that are associated with electron transfer to Q_B in RCs. ENDOR spectroscopy was use to study the H-bond environment near the reduced quinone $Q_B^{-\bullet}$ generated by B-branch electron transfer in the mutant Quint RC that are frozen in the dark (neutral, un-relaxed state) and in the light (charge-separated, relaxed state). The ENDOR spectra in the H-bonding region of $Q_B^{-\bullet}$ formed by B-branch electron transfer in mutant RCs were mostly similar to those in native RCs formed via the conventional A-branch, indicating that $Q_B^{-\bullet}$ was in the proximal active binding position in all cases. We observed one notable difference between the ENDOR spectra of RCs frozen in the light and in the dark. A peak in the H-bonding region of the ^{1}H-ENDOR spectrum was observed in Quint RCs frozen in the light but absent in Quint RCs frozen in the dark. The peak was assigned to an H-bond from Ser L223 on the basis of its absence in Quint RCs carrying the additional mutation Ser L223 → Ala. From these results, we conclude that the H-bond from Ser L223 to $Q_B^{-\bullet}$ is formed upon Q_B reduction.

Although this switch in the H-bond position serves to stabilize the resulting semiquinone, other studies on mutant RCs lacking Ser L223 indicate that the formation of this H-bond is not solely responsible for stabilizing the charge separated state, nor does its absence change the rate-limiting conformational gating step of the Q_B reduction. Rather, the H-bond formation is one of many changes, including protonation events and protein rearrangements, that contribute to charge stabilization and conformational gating. However, the switch of the H-bond from Ser L223 does play a key role in the proton transfer to Q_B. The movement of the Ser L223 H-bond from Asp L213 to $Q_B^{-\bullet}$ serves as the final step in forming an H-bonded chain leading to the protonation of the semiquinone. Several unanswered questions arise from this study. These include the following: What is the rate of the fluctuation of the H-bond? Can H-bond fluctuation be correlated with the gating of electron transfer to Q_B? Future experiments using ENDOR spectroscopy can help to answer these questions.

ACKNOWLEDGMENT

We thank George Feher for helpful discussions.

REFERENCES

1. Sumi, H., and Marcus, R. A. (1986) Dynamic effects in electron-transfer reactions, *J. Chem. Phys. 84*, 4894−4914.
2. Hoffman, B., and Ratner, M. (1987) Gated electron transfer: when are observed rates controlled by conformational interconversion? *J. Am. Chem. Soc. 109*, 6237−6243.
3. Hoffman, B. M., Ratner, M. A., and Wallin, S. A. (1990) Energetics and dynamics of gated reactions- control of observed rates by conformational interconversion, *Adv. Chem. Ser. 226*, 125−146.
4. Blankenship, R. E., Madigan, M. T., and Bauer, C. E. (1995). *Anoxygenic Photosynthetic Bacteria*, Vol. 2, Kluwer Academic Publishers, Dordrecht, The Netherlands.
5. Blankenship, R. E. (2002) *Molecular Mechanisms of Photosynthesis*, Blackwell Science Inc., London.
6. Stowell, M. H., McPhillips, T. M., Rees, D. C., Soltis, S. M., Abresch, E., and Feher, G. (1997) Light-induced structural changes in photosynthetic reaction center: implications for mechanism of electron-proton transfer, *Science 276*, 812−816.
7. Paddock, M. L., Flores, M., Isaacson, R., Chang, C., Abresch, E. C., Selvaduray, P., and Okamura, M. Y. (2006) Trapped conformational states of semiquinone $D^{+\bullet}$ $Q_B^{-\bullet}$ formed by B-branch electron transfer at low temperature in *Rhodobacter sphaeroides* reaction centers, *Biochemistry 45*, 14032−14042.
8. Wraight, C. A. (2004) Proton and electron transfer in the acceptor quinone complex of photosynthetic reaction centers from *Rhodobacter sphaeroides*, *Front. Biosci. 9*, 309−337.
9. Mulkidjanian, A. Y., Kozlova, M. A., and Cherepanov, D. A. (2005) Ubiquinone reduction in the photosynthetic reaction centre of *Rhodobacter sphaeroides*: interplay between electron transfer, proton binding and flips of the quinone ring, *Biochem. Soc. Trans. 33*, 845−850.
10. Noks, P. P., Lukashev, E. P., Kononenko, A. A., Venediktov, P. S., and Rubin, A. B. (1977) Possible role of macromolecular components in functioning of photosynthetic reaction centers of purple bacteria, *Mol. Biol. 11*, 835−842.
11. Francia, F., Palazzo, G., Mallardi, A., Cordone, L., and Venturoli, G. (2003) Residual water modulates Q_A^--to-Q_B electron transfer in bacterial reaction centers embedded in trehalose amorphous matrices, *Biophys. J. 85*, 2760−2775.
12. Francia, F., Giachini, L., Palazzo, G., Mallardi, A., Boscherini, F., and Venturoli, G. (2004) Electron transfer kinetics in photosynthetic reaction centers embedded in polyvinyl alcohol films, *Bioelectrochemistry 63*, 73−77.
13. Graige, M. S., Feher, G., and Okamura, M. Y. (1998) Conformation gating of the electron transfer reaction $Q_A^{-\bullet}Q_B \rightarrow Q_AQ_B^{-\bullet}$, in bacterial reaction centers of *Rb. sphaeroides* determined by a driving force assay, *Proc. Natl. Acad. Sci. U.S.A. 95*, 11679−11684.

14. Chamorovsky, S. K, Remennikov, S. M., Kononenko, A. A., Venediktov, P. S., and Rubin, A. B. (1976) New experimental approach to the estimation of rate of electron transfer from the primary to secondary acceptors in the photosynthetic electron transport chain of purple bacteria, *Biochim. Biophys. Acta 430*, 62−70.
15. Kleinfeld, D., Okamura, M. Y., and Feher, G. (1984) Electron-transfer kinetics in photosynthetic reaction centers cooled to cryogenic temperatures in the charge-separated state: evidence for light-induced structural changes, *Biochemistry 23*, 5780−5786.
16. Weil, J. A., Bolton, J. R., and Wertz, J. E. (1994) *Electron Paramagnetic Resonance. Elementary Theory and Practical Applications*, Wiley, New York.
17. Schweiger, A., and Jeschke, G. (2001) *Principles of Pulse Electron Paramagnetic Resonance*, Oxford University Press, Oxford, U.K.
18. Xu, Q., and Gunner, M. R. (2001) Trapping conformational intermediate states in the reaction center protein from photosynthetic bacteria, *Biochemistry 40*, 3232−3241.
19. Xu, Q., Baciou, L., Sebban, P., and Gunner, M. R. (2002) Exploring the energy landscape for Q_A^- to Q_B electron transfer in bacterial photosynthetic reaction centers: effect of substrate position and tail length on the conformational gating step, *Biochemistry 41*, 10021−10025.
20. Kuglstatter, A., Ermler, U., Michel, H., Baciou, L., and Fritzsch, G. (2001) X-ray structure analyses of photosynthetic reaction center variants from *Rhodobacter sphaeroides*: structural changes induced by point mutations at position L209 modulate electron and proton transfer, *Biochemistry 40*, 4253−4260.
21. Breton, J. (2004) Absence of large-scale displacement of quinone QB in bacterial photosynthetic reaction centers, *Biochemistry 43*, 3318−3326.
22. Paddock, M. L., Chang, C., Xu, Q., Abresch, E. C., Axelrod, H. L., Feher, G., and Okamura, M. Y. (2005) Quinone Q_B reduction by B-branch electron transfer in mutant bacterial reaction centers from *Rhodobacter sphaeroides*: quantum efficiency and X-ray structure, *Biochemistry 44*, 6920−6928.
23. Ridge, J. P., van Brederode, M. E., Goodwin, M. G., van Grondelle, R., and Jones, M. R. (1999) Mutations that modify or exclude binding of the Q_A ubiquinone and carotenoid in the reaction center from *Rhodobacter sphaeroides*, *Photosynth. Res. 59*, 9−26.
24. McAuley, K. E., Fyfe, P. K., Ridge, J. P., Cogdell, R. J., Isaacs, N. W., and Jones, M. R. (2000) Ubiquinone binding, ubiquinone exclusion, and detailed cofactor conformation in a mutant bacterial reaction center, *Biochemistry 39*, 15032−15043.
25. Lubitz, W., and Feher, G. (1999) The primary and secondary acceptors in bacterial photosynthesis: III. Characterization of the quinone radicals $Q_A^{-\bullet}$ and $Q_B^{-\bullet}$ by EPR and ENDOR, *Appl. Magn. Reson. 17*, 1−48.
26. Flores, M., Isaacson, R., Abresch, E., Calvo, R., Lubitz, W., and Feher, G. (2007) Protein-cofactor interactions in bacterial reaction denters from *Rhodobacter sphaeroides* R-26: II. Geometry of the hydrogen bonds to the primary quinine $Q_A^{-\bullet}$ by ^1H and ^2H ENDOR spectroscopy, *Biophys. J. 92*, 671−682.
27. Paddock, M. L., Rongey, S. H., Abresch, E. C., Feher, G., and Okamura, M. Y. (1988) Reaction centers from three herbicide resistant mutants of *Rhodobacter sphaeroides* 2.4.1: sequence analysis and preliminary characterization, *Photosynth. Res. 17*, 75−96.
28. Debus, R. J., Feher, G., and Okamura, M. Y. (1986) Iron-depleted reaction centers from *Rhodopseudomonas sphaeroides* R-26.1: characterization and reconstitution with Fe^{2+}, Mn^{2+}, Co^{2+}, Ni^{2+}, Cu^{2+}, and Zn^{2+}, *Biochemistry 25*, 2276−2287.
29. Utschig, L. M., Greenfield, S. R., Tang, J., Laible, P. D., and Thurnauer, M. C. (1997) Influence of iron-removal procedures on sequential electron transfer in photosynthetic bacterial reaction centers studied by transient EPR spectroscopy, *Biochemistry 36*, 8548−8558.
30. Flores, M., Isaacson, R., Abresch, E., Calvo, R., Lubitz, W., and Feher, G. (2006) Protein-cofactor interactions in bacterial reaction denters from *Rhodobacter sphaeroides* R-26: I. Identification of the ENDOR lines associated with the hydrogen bonds to the primary quinine $Q_A^{-\bullet}$, *Biophys. J. 90*, 3356−3362.
31. Flores, M., Isaacson, R., Calvo, R., Feher, G., and Lubitz, W. (2003) Probing hydrogen bonding to quinone anion radicals by ^1H and ^2H ENDOR spectroscopy at 35 GHz, *Chem. Phys. 294*, 401−413.
32. Sinnecker, S., Flores, M., and Lubitz, W. (2006) Protein-cofactor interactions in bacterial reaction centers from *Rhodobacter sphaeroides* R-26: effect of hydrogen bonding on the electronic and geometric structure of the primary quinone. A density functional theory study, *Phys. Chem. Chem. Phys. 8*, 5659−5670.
33. Butler, W. F., Johnston, D. C., Shore, H. B., Fredkin, D. R., and Feher, G. (1980) The electronic structure of Fe^{2+} in reaction centers from *Rhodopseudomonas sphaeroides*. I. Static magnetization measurements, *Biophys. J. 32*, 967−992.
34. Paddock, M. L., Abresch, E. C., Isaacson, R. A., Feher, G., and Okamura, M. Y. (1997) Identification of hydrogen bonds to $Q_B^{-\bullet}$ in RCs of *Rb. sphaeroides* by ENDOR spectroscopy, *Biophys. J. 72*, A8.
35. Xu, Q., Axelrod, H. L., Abresch, E. C., Paddock, M. L., Okamura, M. Y., and Feher, G. (2004) X-ray structure determination of three mutants of the bacterial photosynthetic reaction centers from *Rb. sphaeroides*: altered proton transfer pathways, *Structure 12*, 703−715.
36. Fritzsch, G., Koepke, J., Diem, R., Kuglstatter, A., and Baciou, L. (2002) Charge separation induces conformational changes in the photosynthetic reaction centre of purple bacteria, *Acta. Crystallogr., Sect. D 58*, 1660−1663.
37. Creighton, T. E. (1993) *Proteins: Structures and Molecular Properties*, W. H. Freeman & Co., New York.
38. Utschig, L. M., Thurnauer, M. C., Tiede, D. M., and Poluektov, O. G. (2005) Low-temperature interquinone electron transfer in photosynthetic reaction centers from *Rhodobacter sphaeroides* and *Blastochloris viridis*: characterization of Q_B^- states by high-frequency electron paramagnetic resonance (EPR) and electron-nuclear double resonance (ENDOR), *Biochemistry 44*, 14131−14142.
39. Paddock, M. L., McPherson, P. H., Feher, G., and Okamura, M. Y. (1990) Pathway of proton transfer in bacterial reaction centers: replacement of serine-L223 with alanine inhibits electron and proton transfers associated with reduction of quinone to dihydroquinone, *Proc. Natl. Acad. Sci. U.S.A. 87*, 6803−6807.
40. McMahon, B. H., Muller, J. D., Wraight, C. A., and Nienhaus, G. U. (1998) Electron transfer and protein dynamics in the photosynthetic reaction center, *Biophys. J. 74*, 2567−2587.
41. Xu, Q., and Gunner, M. R. (2002) Exploring the energy profile of the Q_A^- to Q_B^- electron transfer reaction in bacterial photosynthetic reaction centers: pH dependence of the conformational gating step, *Biochemistry 41*, 2694−2701.
42. Marcus, R. A., and Sutin, N. (1985) Electron transfer in chemistry and biology, *Biochim. Biophys. Acta 811*, 265−322.
43. Alexov, E. G., and Gunner, M. R. (1999) Calculated protein and proton motions coupled to electron transfer: electron transfer from Q_A^- to Q_B in bacterial photosynthetic reaction centers, *Biochemistry 38*, 8253−8270.
44. Ishikita, H., and Knapp, E-W. (2004) Variation of Ser-L223 hydrogen bonding with the Q_B redox state in reaction centers from *Rhodobacter sphaeroides*, *J. Am. Chem. Soc. 126*, 8059−8064.
45. Zhu, Z., and Gunner, M. R. (2005) Energetics of quinone-dependent electron and proton transfers in *Rhodobacter sphaeroides* photosynthetic reaction centers, *Biochemistry 1*, 82−96.
46. Hermes, S., Stachnik, J. M., Onidas, D., Remy, A., Hofmann, E., and Gerwert, K. (2006) Proton uptake in the reaction center mutant L210DN from *Rhodobacter sphaeroides* via protonated water molecules, *Biochemistry 45*, 13741−13749.
47. Nabedryk, E., Paddock, M. L., Okamura, M. Y., and Breton, J. (2005) An isotope-edited FTIR investigation of the role of Ser-L223 in binding quinone Q_B and semiquinone Q_B^- in the reaction center from *Rhodobacter sphaeroides*, *Biochemistry 44*, 14519−14527.
48. Takahashi, E., and Wraight, C. (1992) Proton and electron transfer in the acceptor quinone complex of *Rhodobacter sphaeroides* reaction centers: characterization of site-directed mutants of the two ionizable residues, GluL212 and AspL213, in the Q_B binding site, *Biochemistry 31*, 855−866.
49. Paddock, M. L., Rongey, S. H., McPherson, P. H., Juth, A., Feher, G. and Okamura, M. Y. (1994) Pathway of proton transfer in bacterial reaction centers: role of aspartate-L213 in proton transfer associated with reduction of quinone to dihydroquinone, *Biochemistry 33*, 734−745.
50. Nabedryk, E., Breton, J., Hienerwadel, R., Fogel, C., Mantele, W., Paddock, M. L., and Okamura, M. Y. (1995) Fourier transform infrared difference spectroscopy of secondary quinone acceptor photoreduction in proton transfer mutants of *Rhodobacter sphaeroides*, *Biochemistry 34*, 14722−14732.

51. Nagle, J. F., and Tristram-Nagle, S. (1983) Hydrogen bonded chain mechanisms for proton conduction and proton pumping, *J. Membr. Biol. 74*, 1−14.
52. Graige, M. S., Paddock, M. L., Bruce, J. M., Feher, G., and Okamura, M. Y. (1996) Mechanism of proton-coupled electron transfer for quinone Q_B reduction in reaction centers of *Rb. sphaeroides*, *J. Am. Chem. Soc. 118*, 9005−9016.
53. Okamura, M. Y., Paddock, M. L., Graige, M. S., and Feher G. (2000) Proton and electron transfer in bacterial reaction centers, *Biochim. Biophys. Acta 1458*, 148−163.
54. Lancaster, C. R. D., and Michel, H. (1997) The coupling of light-induced electron transfer and proton uptake as derived from crystal structures of reaction centres from *Rhodopseudomonas viridis* modified at the binding site of the secondary quinone, Q(B), *Structure 5*, 1339−1359.
55. Paddock, M. L., Feher, G., and Okamura, M. Y. (2003) Proton transfer pathways and mechanism in bacterial reaction centers, *FEBS Lett. 555*, 45−50.

BI7005256